Int J Plant Anim Environ Sci 2020; 10 (1): 035-053

Research Article

Distribution of Water and Salt Ions in a Saline–Alkali Wheat Field under Freeze–Thaw Conditions

Li Xiaoshuang[1,3], Dang Hongkai[2], Song Ni[1], Feng Di[4], Sun Jingsheng[1*]

[1]Farmland Irrigation Research Institute, Chinese Academy of Agricultural Sciences, Xinxiang, China

[2]Dryland Farming Institute, Hebei Acadamy of Agricultural and Forestry Sciences, Hengshui, China

[3]Graduate school of Chinese academy of agricultural sciences, Beijing, China

[4]Facility Horticulture Laboratory of Universities in Shandong, Weifang University of Science and Technology, Shandong, Weifang, 262700, China

***Corresponding Author:** Sun Jingsheng, Farmland Irrigation Research Institute, Chinese Academy of Agricultural Sciences, Xinxiang, China, E-mail: jshsun623@163.com

Received: 11 December 2019; **Accepted:** 17 January 2020; **Published:** 25 February 2020

Citation: Li Xiaoshuang, Dang Hongkai, Song Ni, Feng Di, Sun Jingsheng. Distribution of Water and Salt Ions in a Saline–Alkali Wheat Field under Freeze–Thaw Conditions. International Journal of Plant, Animal and Environmental Sciences 10 (2020): 035-053.

Abstract

In order to make clear the distribution characteristics of soil, water and salt in a saline–alkali wheat field under freeze–thaw conditions, field experiment was conducted in Cangzhou during 2015 to 2018. The experiment were selected three key periods, early stage (December 13) and late stage (March 3) of freeze–thaw period, and salt accumulation stage (April 1). The distribution of soil salt ions prior to sowing was regarded as the background. Results showed that the spatial distribution of soil moisture in the 0–100 cm soil layer varied in the different periods. In the early stage of the freeze–thaw period, the soil moisture content decreased with the increase of soil depth in 0-40 cm soil layer, and then increased with the increase of soil depth. The minimum moisture content was found in the 30–40 cm soil layer. Soil electrical conductivity (EC) in the 20–30 cm soil layer was higher than that in other soil layers. Meanwhile, soil pH value increased with the increase in soil depth. SO_4^{2-}, Ca^{2+}, Cl^- and Mg^{2+} all aggregated to the surface. After freezing and thawing, the moisture content in the 0–60 cm soil layer increased with the increase in soil depth. The moisture content dropped

precipitously in the 60–80 cm soil layer, and then the moisture content quickly rebounded to the soil layer below 80 cm. Soil EC increased with the increase of soil depth. With increase depth of soil layer, the pH value appeared peak in the 10-30 cm soil layer and then decreases. The pH value of the soil below 40 cm gradually increased with the increase of soil depth. SO_4^{2-}, Ca^{2+}, Mg^{2+} and Na^+ showed a trend of large at surface and deep soil layers, and samll in the middle soil layer. HCO_3^- accumulates at 0-30 cm soil layer. Cl^- was increase with the increase of soil layer. During the salt accumulation period, the moisture content in the 0–20 cm soil layer was significantly lower than that in the soil layer below 20 cm. Various ions accumulated in the 0–20 cm soil layer, and the soil EC was also significantly higher than that in the soil layer below 20 cm. At this period, roots of wheat were densely distributed in the 0-20 cm soil layer. Therefore, timely irrigation could alleviate the dual stress of drought and salt damage on winter wheat. The redistribution characteristics of water and salt ions before and after the freeze–thaw period could be used as the theoretical basis for the prevention and improvement of salinised soil.

Keywords: Saline–alkali wheat field; Freezing and thawing; Soil moisture; Salt ion

1. Introduction

For decades, research had shown that the freeze–thaw cycle was a process of energy input and output in soil. Such cycle had a crucial effect on the pore water of seasonal frozen soil (Ren *et al.*, 2019). Soil water expanded under the action of crystallisation and promotes the formation of soil structure through the movement of water and salt via thermal gradient. Soil structure changed greatly after a freeze–thaw cycle; such change was caused by the mechanical breaking of coarse mineral particles and the aggregation of fine particles (Zhang *et al.*, 2016). During the seasonal freeze–thaw process, soil aggregates destroy and change the soil structure, resulting in the soil pore space to shrink and expand during water phase transition (Li *et al.*, 2014); thus, soil porosity improved remarkably (Chen *et al.*, 2010). The physical properties of soil, such as compactness, bulk density, saturated hydraulic conductivity and infiltration rate, were altered due to the changes in soil structure (Asare *et al.*, 1999; Fouli *et al.*, 2013). The seasonal freeze–thaw cycle could reduce the compaction of farmland saline soil, improve soil aeration and retain soil moisture (Wang *et al.*, 2020). Asarea et al. (1999) found that saturation degree was negatively correlated with soil electrical conductivity (EC) values after multiple freeze–thaw cycles on three different soil types—silty loam, clay loam and loam sand. The freeze–thaw process could considerably change the soil carbon and nitrogen cycle and reduce microbial nitrogen- and microbial carbon-to-nitrogen ratio. An increase in the content of dissolved organic carbon and nitrogen in soil and in the concentration of NH_4^+, NO_3^- and soluble inorganic nitrogen (Song *et al.*, 2017; Claudia *et al.*, 2017) and a large part of the emissions can occur during the freeze–thaw cycle (Wertz *et al.*, 2016). Nitrogen deposition delays peak soil respiration during the spring freeze–thaw period and weakens soil respiration (Yan *et al.*, 2016).

Soil salinisation was one of the obstacles to the sustainable development of society, economy and environment (Tilman *et al.*, 2002; Spiess *et al.*, et al.; 2008; Bryan *et al.*, 2018). The law of water and salt migration was the theoretical basis for studying the mechanism of salt soil development and utilisation (Zhang *et al.*, 2017). Factors that affected the properties of saline soil include water, heat, salt and force. Water movement was a dominant factor. In addition to water potential gradient, temperature gradient was another

driving force of water and salt movement in winter. The amount of water and salt migration depended on the total soil water content. In winter, groundwater was buried shallowly. The surface water carried salt rising under capillary force or freezing action, and the salt remains on the surface after evaporation (Warren *et al.*, 2016). In the natural environment, when the temperature droped below negative temperature, water and salt gather towards the surface (Chapra *et al.*, 1997). Soil water and salt moved twice as fast during the freeze–thaw period (Edwards *et al.*, 1992). The characteristics varied at different stages. During the freeze–thaw period, salt ions migrate to the frozen zone with the increased in the matrix potential at the frozen edge (Angela *et al.*, 2016). During thawing, unmelted ice blocked the upper melted water, which carried salt downwards for infiltration. The retained water and salt migrate to the surface and evaporate under the influence of temperature, thus increasing the surface salt (He *et al.*, 2015) in areas with latitudes higher than 24°. In China, more than half of the national land was covered by seasonal frozen soil (Xu *et al.*, 2010). Northwest China had many arid irrigation areas, e.g. the North China Plain. Hebei Province is located northeast of the North China Plain. Its saline soil area was 4.96×10^5 hm^2, accounting for 8.43% of the total cultivated area of the entire province (Guo *et al.*, 2012). Many scholars had conducted substantial research on the improvement, development and utilisation of saline soil in the North China Plain (Scott *et al.*, 1997; Ma *et al.*, 2008; Shi *et al.*, 2019); however, reports on the mechanism of water and salt migration in a salinised wheat field under freezing and thawing conditions were rarely reported.

The influence of the freeze–thaw process on soil structure was determined by soil water content, soil salinity, land surface temperature and other factors (Yi *et al.*, 2014; Wu *et al.*, 2015; Miao *et al.*, 2017). However, the distribution of water and salt and the freeze–thaw mechanism in a vertical soil profile when soil texture changes with time were not clear. Therefore, the distribution of water and salt ions was observed for three years before and after the seasonal freeze–thaw process in Nanpi County, Hebei Province, China, which had a typical salinised soil. This study aimed to explore the water and salt transport mechanism during the freeze–thaw process, and provided a theoretical basis for salinisation prevention, development and utilisation.

2. Materials and methods

2.1 Condition of the test area

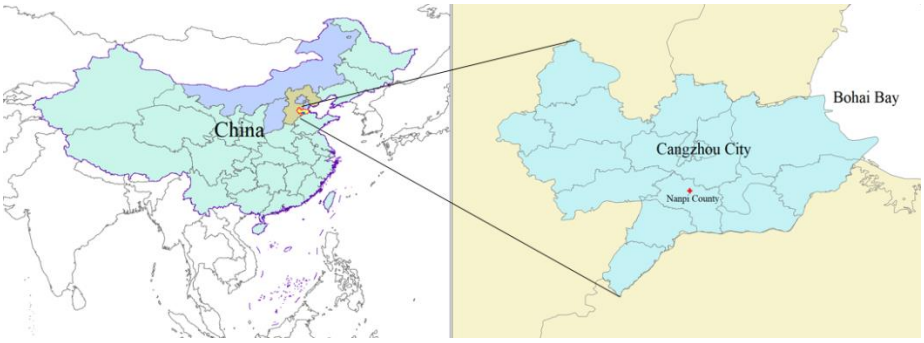

Figure 1: Location of the test area

The field experiment was conducted at Musanbo Farm in Nanpi County, Hebei Province, China (38° 06′ N, 116° 77′ E; 9.5 m above sea level) during 2015 to 2018. The test area is located in the low coastal plain near the southeast of Hebei Province, belonging to the alluvial plain of the Yellow and Haihe Rivers (Figure. 1). The climate belongs to the warm temperate semihumid continental monsoon. The annual average temperature, rainfall, evaporation and frost-free period are 12.3℃, 550 mm, 1865 mm and 180 days, respectively (meteorological data of Nanpi County for 60 consecutive years from 1956 to 2015 [Table 1]). The depth of groundwater was 3.89–6.71 m from 2015 to 2018. The planting system in this area is two crops per year, that is, wheat in winter and corn in summer. We analysed the salinity and nutrient status of the cultivated soil layer before sowing winter wheat (October 3, 2015). Data are as follows: soil salinity of 1.2–2.8 $g \cdot kg^{-1}$, soil organic matter of 1.19–1.30 $g \cdot kg^{-1}$ at the 0–20 cm soil layer, total nitrogen of 79–86 $mg \cdot kg^{-1}$, available nitrogen of 49–53 $mg \cdot kg^{-1}$, available phosphorus of 6.2–6.9 $mg \cdot kg^{-1}$ and available potassium of 125–130 $mg \cdot kg^{-1}$. The soil is alluvial, and its characteristics are shown in Table 2.

Seasons	Rainfall (mm)						
	October	November	December	January	February	March	Total
2015/2016	25.8	55.5	0.3	2.4	27.7	0	111.7
2016/2017	72.6	22.4	18.2	0	7.8	18.8	139.8
2017/2018	80.4	0	0.2	1.8	0	2.6	85.0
Average of 1967–2015	28.8	11.8	4.2	3.3	7.1	9.4	64.6

Table 1: Monthly precipitation for the experimental periods of winter wheat in 2015–2018 and the long-term average.

Soil depth (cm)	pH	Texture	BD (g/cm^3)	FC (vol %)	WP (vol %)	$EC_{1:5}$ (ds/m)	Ion composition (g/kg)					
							HCO_3^-	Cl^-	SO_4^{2-}	Ca^{2+}	Mg^{2+}	Na^+
0–10	8.50	Light loam	1.40	34.2	9.9	3.05	0.480	0.230	0.310	0.060	0.060	0.310
10–20	8.55	Light loam	1.40	34.2	9.9	3.25	0.480	0.260	0.330	0.050	0.050	0.350
20–30	8.60	Medium loam	1.46	34.4	11.6	3.35	0.500	0.266	0.432	0.055	0.062	0.385
30–40	8.55	Medium loam	1.46	34.4	11.6	3.50	0.480	0.300	0.468	0.055	0.067	0.414
40–50	8.60	Medium loam	1.46	34.4	11.6	3.45	0.480	0.260	0.432	0.060	0.062	0.385
50–60	8.65	Medium loam	1.46	34.4	11.6	3.75	0.440	0.330	0.492	0.050	0.050	0.466
60–70	8.65	Silt clay	1.49	37.8	13.9	4.30	0.450	0.360	0.384	0.055	0.056	0.443
70–80	8.60	Silt clay	1.49	37.8	13.9	5.50	0.440	0.390	0.528	0.075	0.062	0.500
80–90	8.65	Silt clay	1.49	37.8	13.9	5.90	0.420	0.440	0.612	0.075	0.068	0.506
90–100	8.75	Silt clay	1.49	37.8	13.9	5.90	0.440	0.410	0.600	0.075	0.078	0.431

BD: bulky density; FC: field capacity; WP: wilting point

Table 2: Background value of soil characteristics at the test area

2.2 Sample collection

The sampling periods were as follows: before wheat sowing (October 3), the early (December 13) and late (March 3 of the following year) stages of the freeze–thaw period and the salt accumulation period (April 1); these periods were denoted as BS, EFT, LFT and SA, respectively. The experimental area was 120×30 m. The S-shaped equidistant sampling method was used, with three samples taken at each time. The sampling depths were 0–10, 10–20, 20–30, 30–40, 40–50, 50–60, 60–80 and 80–100 cm. The samples for analysis were placed in the shade dry naturally after retrieval from soil and then placed in a self–sealing bag after electric grinding using a 1 mm sieve.

2.3 Measurement index and calculation method

The volume moisture content was calculated in accordance with the following formula:

$$\theta_g = \frac{M - M_a}{M_a} \times 100\% \quad \text{(Eq. 1)}$$

$$\theta_v = \frac{\rho_d}{\rho_w} \times \theta_g \quad \text{(Eq. 2)}$$

where θ_g is soil mass moisture content, %; M is original soil weight, g; M_a is dry soil weight, g; θ_v is volume moisture content of soil, %; ρ_w is water density, $g \cdot cm^{-3}$; ρ_d is soil dry bulk density, $g \cdot cm^{-3}$. The dry bulk density of different soil layers is shown in Table 2.

The pH value of soil was determined using a pH meter. The total water-soluble salt content was determined via conductometry (soil-to-water ratio of 5:1). Bicarbonate was titrated using a double-indicator neutralisation method. The chloride ions were titrated with silver nitrate. Indirect complexometric titration with Ethylene Diamine Tetraacetic Acid complexometric method (EDTA) was used for sulphuric acid. Calcium and magnesium were titrated with EDTA. Sodium and potassium ions were determined via flame photometry. The concentration of potassium ions is low in water; thus, it was calculated as sodium ions. The value of Cl^-/SO_4^{2-} is the molar equivalent ratio of Cl^- to SO_4^{2-} (Bao, 2000).

Sodium adsorption ratio (SAR) is an index reflecting the change in soil quality during saline–alkali land improvement. The SAR described in this study was based on an extract with a soil-to-water ratio of 5:1. The calculation formula is as follows (Mohsen *et al*., 2009):

$$SAR=[Na^+]/\sqrt{([Ca^{2+}]+[Mg^{2+}])/2} \quad \text{(Eq. 3)}$$

where SAR is sodium adsorption ratio, $(cmol\cdot kg^{-1})^5$; Na^+, Ca^{2+} and Mg^{2+} are measured exchangeable Na^+, Ca^{2+} and Mg^{2+}, respectively, $cmol\cdot kg^{-1}$.

2.4 Data statistics and analysis

Excel 2010, SigmaPlot 12.5 and SPSS 19.0 were used for data entry and analysis, scientific plotting and significant difference analysis, respectively.

3. Result and Analysis

3.1 Characteristics of soil water distribution

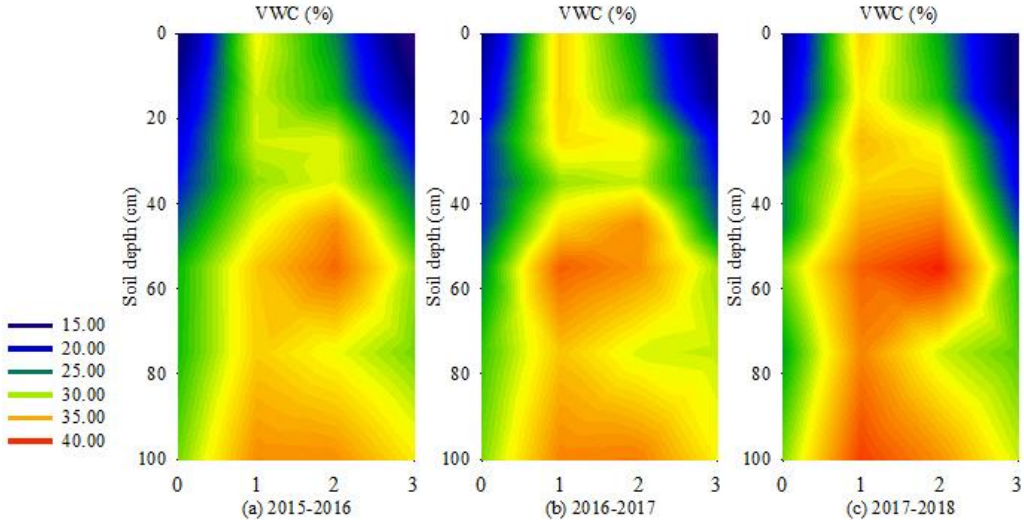

Figure 2: Change of soil moisture in the 0–100 cm soil profile in 2015–2018

The abscissa represents the sampling period. 0- BS (October 3); 1- EFT (December 3); 2- LFT (March 3 of the following year); 3- SA (April 1 of the following year). The same was shown below. Figure.1 showed the volume moisture content of each period from 2015 to 2018. The volume moisture content of BS increased with the depth of soil layer, and the variation range was 14.85%–28.85%. The water content of the soil volume of EFT was distributed in an upward direction with the 30–40 cm soil layer as the dividing line; this distribution showed a trend of large at surface and deep soil layers and small in the middle, and the water content was significantly higher than that of BS. The volumetric water content in the 30–40 cm soil layer varied from 29.25% to 31.96%, which was 5.88% lower than that in the upper layer and 7.73% lower than that in the lower layer. The volumetric moisture content of other soil layers ranged from 30.48% to 39.06%. The moisture content of LFT increased with soil depth in the 0–60 cm soil layer, and the volume moisture content of the 60–80 cm soil layer decreased rapidly. Compared different soil layers under same time , the average moisture content of the 60–80 cm soil layer lower than 60–80 cm 14.16%, and the 80–100 cm higher than 60-80 cm soil layer 14.62%. The volumetric moisture content of SA increased with soil depth. The moisture content in the 0–20 cm soil layer was significantly lower than that in the soil layer below 20 cm, varying between 12.93% and 15.15%. Comparing between years, the moisture content of EFT showed the order 2018 > 2017 > 2016 in the 0–100 cm soil layer.

3.2 Characteristics of soil EC distribution

The change of soil EC can directly reflect the change of soil salinity (Figure 3). The EC average of BS was lower (3.7–6.1 $ds \cdot m^{-1}$) in the 0–100 cm soil layer. It reached the maximum value (4.7–6.1 $ds \cdot m^{-1}$) in EFT or LFT and decreased in SA (4.4–5.0 $ds \cdot m^{-1}$). The EC of BS increased with the increase in soil depth (2.5–6.1 $ds \cdot m^{-1}$). The EC of EFT in the 20–30 cm soil layer was the largest (5.5–8.3 $ds \cdot m^{-1}$), and the soil layer below 40 cm increased with the increase in soil depth (3.6–6.5 $ds \cdot m^{-1}$). The EC of LFT increased with the increase in soil depth (3.3–6.0 $ds \cdot m^{-1}$). The EC values of SA were relatively high in the 0–20 cm (4.5–6.9 $ds \cdot m^{-1}$) and below 60 cm (4.6–5.6 $ds \cdot m^{-1}$) soil layers. Comparing the average EC values of the 0–100 cm soil layer each year revealed the following orders: 2016 < 2017 < 2018 in BS, 2018 < 2017 < 2016 in EFT, 2017 < 2018 < 2016 in LFT and 2017 < 2016 < 2018 in SA.

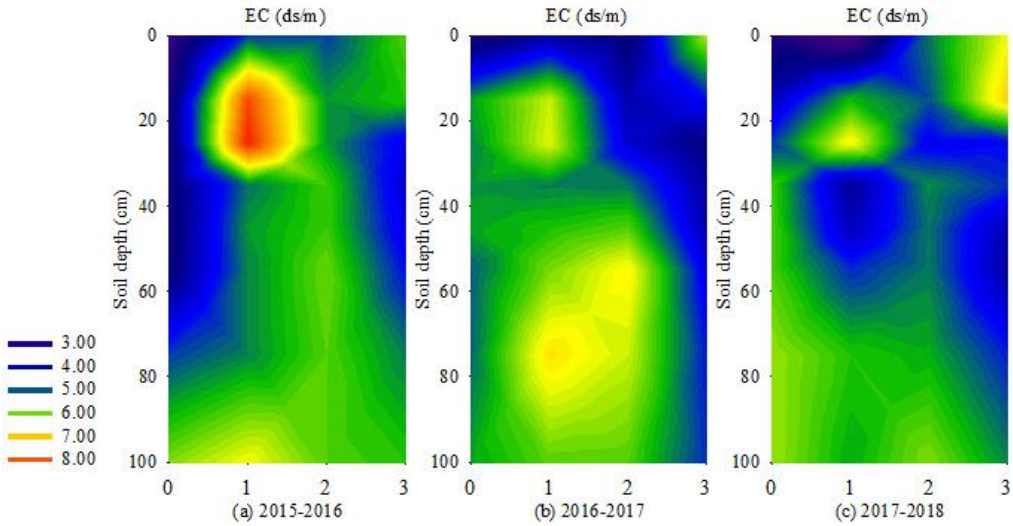

Figure 3: Soil EC in the 0–100 cm soil profile in 2015–2018

3.3 pH change at the 0–100 cm soil layer

The pH value in the 0–100 cm soil layer during 2015–2018 varied in different periods, as shown in Figure.3. The pH value of BS was the smallest (8.52–8.59), increased in EFT (8.60–8.66), decreased in LFT (8.55–8.60) and increased again in SA (8.63–8.65). The pH value increased with the increase in soil depth in BS and EFT (the variation range was 8.50–8.90 and 8.50–8.70, respectively). The pH value of LFT (8.64–8.70) was higher than that of other soil layers in the 10–30 cm soil layer, and the pH value increased with soil depth in the soil layer below 30 cm. The pH value of SA was high in the 20–30 cm or 30–40 cm soil layers (8.70–8.74), indicating that the mean pH value of the entire section decreased with the age compared between years.

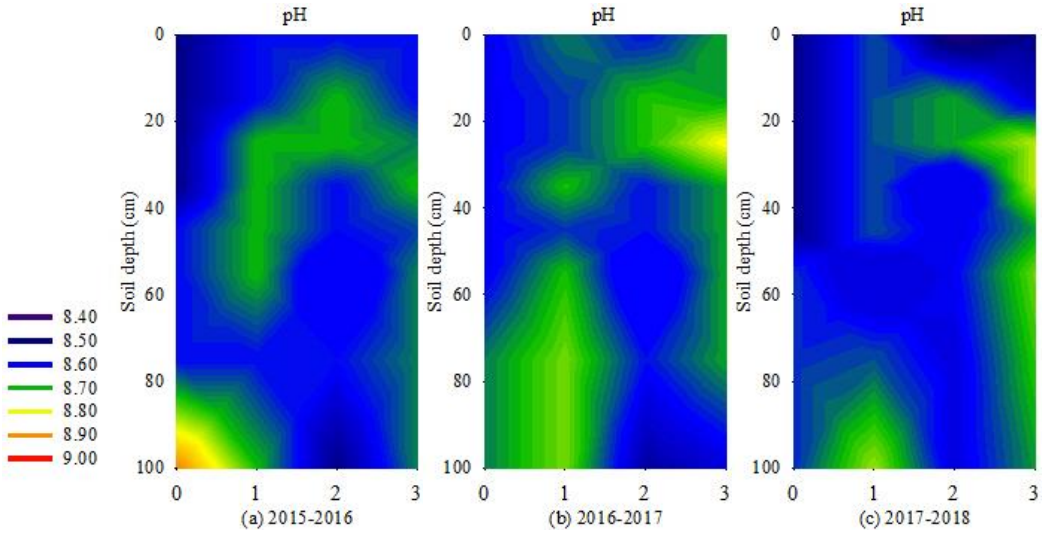

Figure 4: Changes of pH value in the 0–100 cm soil profile in 2015–2018

3.4 Characteristics of soil anion distribution

3.4.1 HCO_3^- distribution: HCO_3^- distribution in the 0–100 cm soil layer from 2015 to 2018 is shown in Figure.5 (a1), (b1) and (c1). The HCO_3^- content of BS was relatively evenly distributed in the 0–100 cm soil layer. The HCO_3^- content of EFT accumulated in the 50–80 cm soil layer (0.457–0.505 g·kg^{-1}). Meanwhile, that of LFT was high and concentrated (0.366–0.583 g·kg^{-1}) in the 0–30 cm soil layer, and that of SA accumulated in the 20–60 cm soil layer (0.406–0.518 g·kg^{-1}). A comparison amongst the three years showed that the HCO_3^- content was the highest in the 0–100 cm soil layer in 2016-2017 during the sowing period. It was the highest among three years that the HCO_3^- content of LFT in the 0-100 cm soil layer in 2017-2018 and so did SA. All were due to HCO_3^- easily dissolved in water and migrates with water movement. The varying precipitation distribution from September to April of the next year leads to different contents in the 0–100 cm soil layer. This difference was due to the different precipitation distribution (Table 1) in each experimental period.

3.4.2 Cl^- distribution: Cl^- distribution in the 0–100 cm soil layer from 2015 to 2018 is shown in Figure.4 (a2), (b2) and (c2). The Cl^- distribution of each treatment changes were different in the 0-100cm profile The Cl^- content of BS increased with the increase in soil depth in the 0–100 cm soil layer. The Cl^- content of EFT was high in the 10–40 (0.319–0.780 g·kg^{-1}) and 80–100 cm (0.354–0.602 g·kg^{-1}) soil layers. The Cl^- content of LFT increased with soil depth in the 0–100 cm soil layer. The Cl^- content of SA accumulated in the 0–20 cm (0.348–0.571 g·kg^{-1}) and below 60 cm (0.392–0.460 g·kg^{-1}) soil layers.

3.4.3 SO_4^{2-} distribution: Figure.4(a3), (b3) and (c3) show the SO_4^{2-} content in the 0–100 cm soil layer from 2015 to 2018. In general, sulphates were significantly affected by water movement because they were easily soluble in water. The SO_4^{2-} content of BS increased with soil depth (0.164–0.528 g·kg^{-1}). The SO_4^{2-} content of EFT accumulated in the 10–30 (0.504–0.696 g·kg^{-1}) and 50–60 cm (0.504–0.552 g·kg^{-1}) soil layers. The SO_4^{2-} content of LFT accumulated in the 20–40 (0.399–0.648 g·kg^{-1}) and 80–100 cm (0.528–0.580 g·kg^{-1}) soil layers. The SO_4^{2-} content of SA accumulated in the 0–20 cm soil layer (0.336–0.528 g·kg^{-1}). The SO_4^{2-} content in the 0–100 cm soil layer decreased every year.

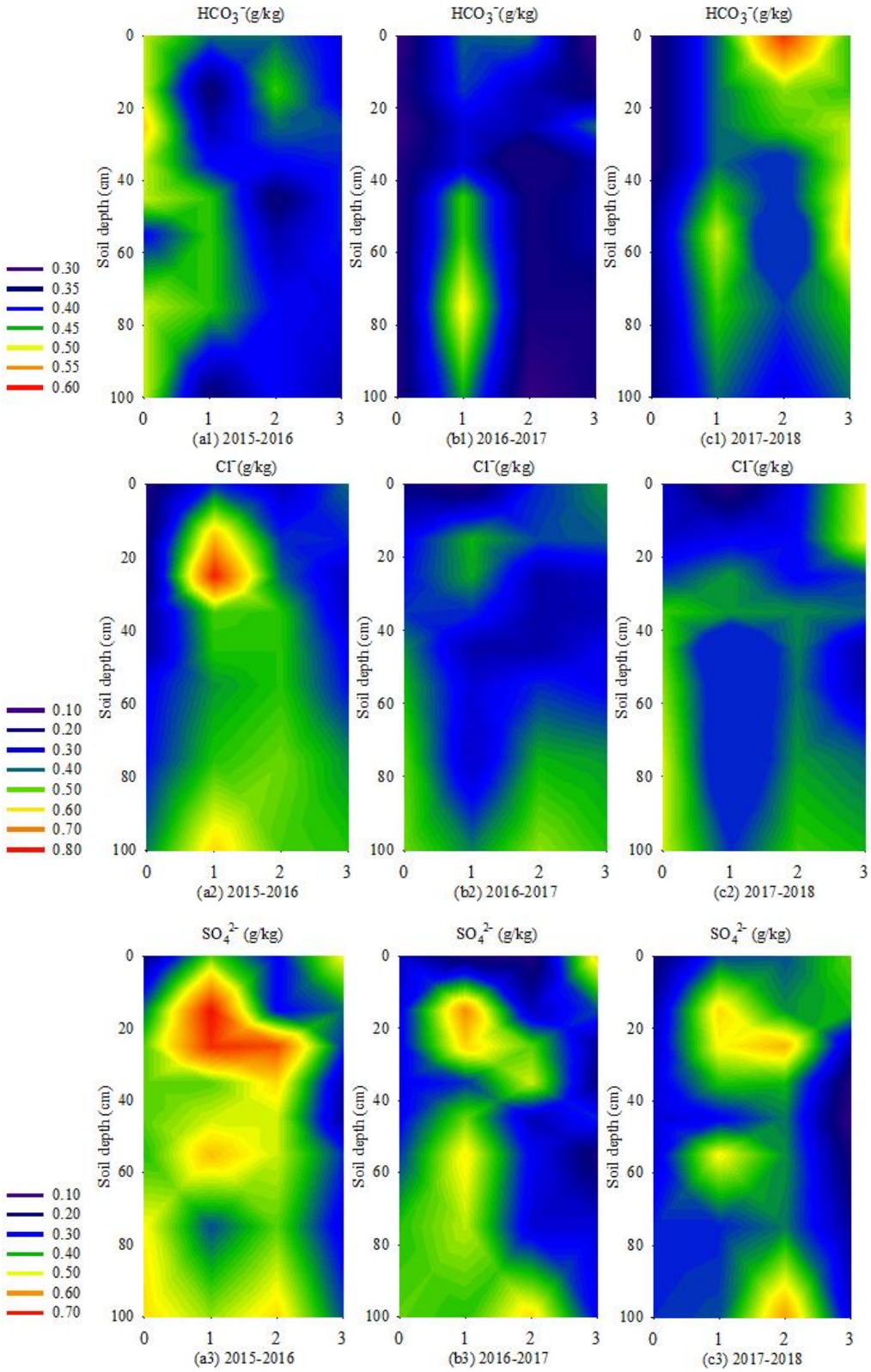

Figure 5: Distribution of anions in the 0–100 cm soil profile in 2015–2018

3.4.4 Change in Cl^-/SO_4^{2-} ratio: In this study, 2015-2016 was selected as the representative year to analyse the changes of Cl^-/SO_4^{2-} in the 0–100 cm soil layer (Table 3). Cl^-/SO_4^{2-} ratios had significant differences ($P < 0.05$) in the 10–20, 20–30, 50–60 and 60–80 cm soil layers. Cl^-/SO_4^{2-} ratios of BS, EFT, LFT and SA were 0.61–1.24, 1.24–2.04, 0.81–1.81 and 1.06–2.54, respectively. Cl^- and SO_4^{2-} were redistributed after the freeze–thaw cycle and reached the highest in SA after soil thaw. The Cl^-/ SO_4^{2-} ratio of SA was relatively large in the 40–80 cm soil layer because the increase in Cl^- amplitude was much higher than that of SO_4^{2-} when Cl^- and SO_4^{2-} increased in this soil layer.

Soil depth (cm)	BS	EFT	LFT	SA	SD	Sig. (2)	t
0-10	1.24	1.57	1.94	1.06	0.37059	0.820	-0.234
10-20	0.73	1.24	1.67	1.34	0.43090	0.253	-1.206
20-30	0.61	1.57	0.81	1.15	0.51448	0.124	-1.666
30-40	0.61	1.57	1.81	1.15	0.58075	0.674	-0.432
40-50	0.72	1.30	1.30	2.00	0.63293	0.901	-0.128
50-60	1.06	2.04	1.63	2.54	0.67028	0.227	1.279
60-80	0.90	1.86	1.55	2.28	0.59494	0.357	0.961
80-100	1.04	1.79	1.23	1.86	0.42617	0.516	0.671

BS: Before winter wheat sowing EFT: The early of freeze-thaw stage; LFT: The late of freeze-thaw stage; SA: the salt accumulation period; SD: Standard deviation; Sig. (2): Probability of two–sided test; t: The statistics of the test.

Table 3: Changes of Cl^-/SO_4^{2-} ratio and its difference significance test in different soil layers

3.5 Soil cation distribution characteristics

3.5.1 Ca^{2+} distribution: Calcium ions could promote soil colloid condensation, which was conducive to the aggregate formation. These ions could also supply the required calcium elements and thus were conducive to crop growth. Figure.5 (a1), (b1) and (c1) showed the Ca^{2+} content distribution in each period from 2015 to 2018. The Ca^{2+} content of EFT accumulated in the 20–30 cm soil layer (0.090–0.150 $g \cdot kg^{-1}$); that of LFT accumulated in the 20–40 (0.070–0.096 $g \cdot kg^{-1}$) and 80–100 cm (0.070–0.100 $g \cdot kg^{-1}$) soil layers; that of SA accumulated in the 0–20 cm soil layer (0.0800–0.114 $g \cdot kg^{-1}$). This result showed that the average Ca^{2+} content in the 0–100 cm soil layer peaked in 2015-2016 and 2016-2017 in EFT (0.084 and 0.089 $g \cdot kg^{-1}$, respectively). However, the peak value appeared in the LFT period (0.079 $g \cdot kg^{-1}$) in 2017-2018.

3.5.2 Mg^{2+} distribution: Mg^{2+} distribution in the 0–100 cm soil layer from 2015 to 2018 was shown in Figure.5 (a2), (b2) and (c2). The Mg^{2+} content of BS accumulated in the 30–40 (0.042–0.066 $g \cdot kg^{-1}$) and 60–100 cm (0.039–0.070 $g \cdot kg^{-1}$) soil layers. In EFT, deep layers accumulation (0.054–0.100 $g \cdot kg^{-1}$) in the soil layer below 50 cm and surface accumulation (0.052–0.121 $g \cdot kg^{-1}$) in the 0–20 cm soil layer occurred. In LFT, Mg^{2+} accumulated in the 20–40 cm

soil layer (0.060–0.115 g·kg^{-1}). The average annual value of Mg^{2+} varied from year to year in the 0–100 cm soil layer; in 2017-2018, it reached the peak in SA.

3.5.3 Na^{+} distribution: Na^{+} distribution in the 0–100 cm soil layer from 2015 to 2018 was shown in Figure.5 (a3), (b3) and (c3). In EFT, medium aggregates were found in the 20–40 (0.383–0.575 g·kg^{-1}) and 80–100 cm (0.402–0.494 g·kg^{-1}) soil layers. In LFT, surface and deep layer accumulation occurred in the 30–40 (0.402–0.483 g·kg^{-1}) and 60–100 cm (0.368–0.498 g·kg^{-1}) soil layers, respectively. The surface accumulation of SA occurred in the 0–20 cm soil layer (0.421–0.511 g·kg^{-1}), whereas deep layer accumulation occurred in the 60–100 cm soil layer (0.402–0.434 g·kg^{-1}).

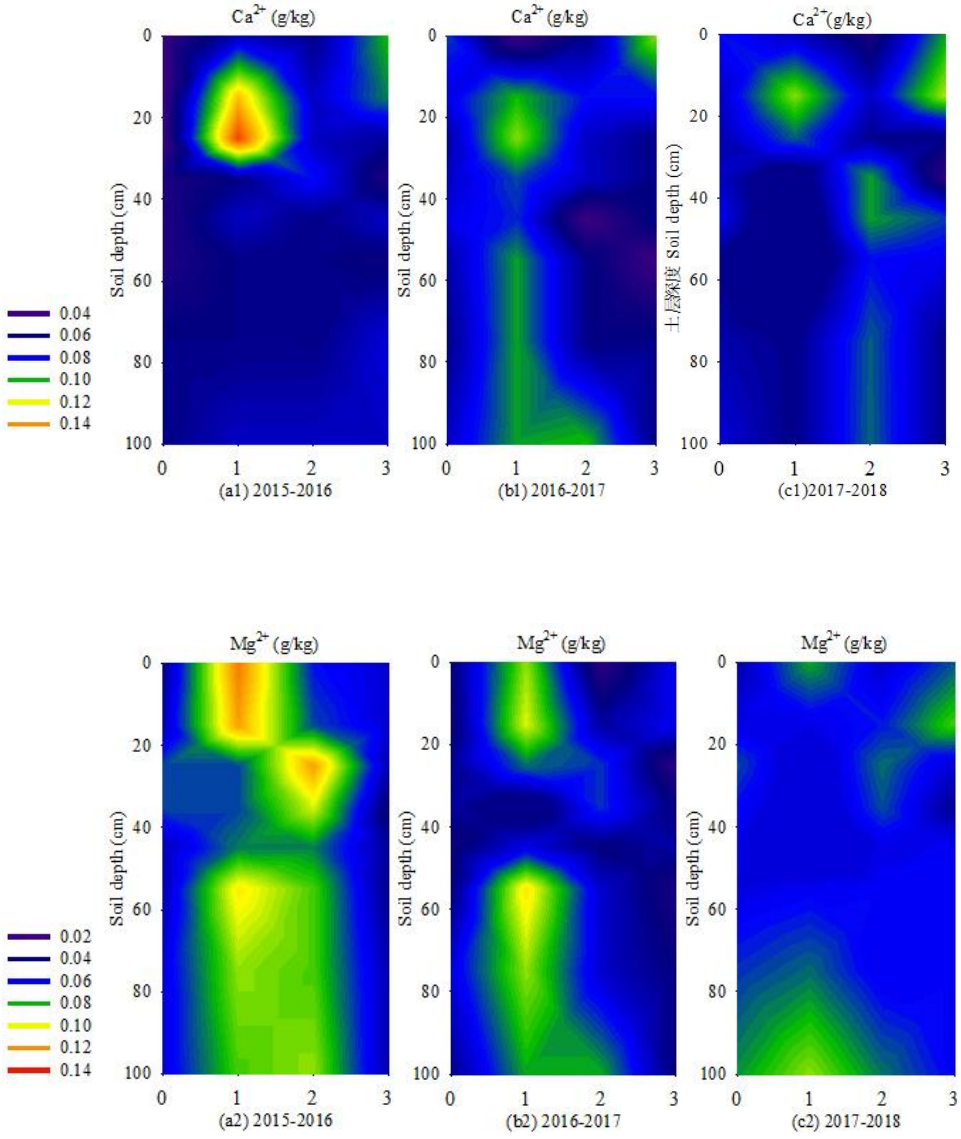

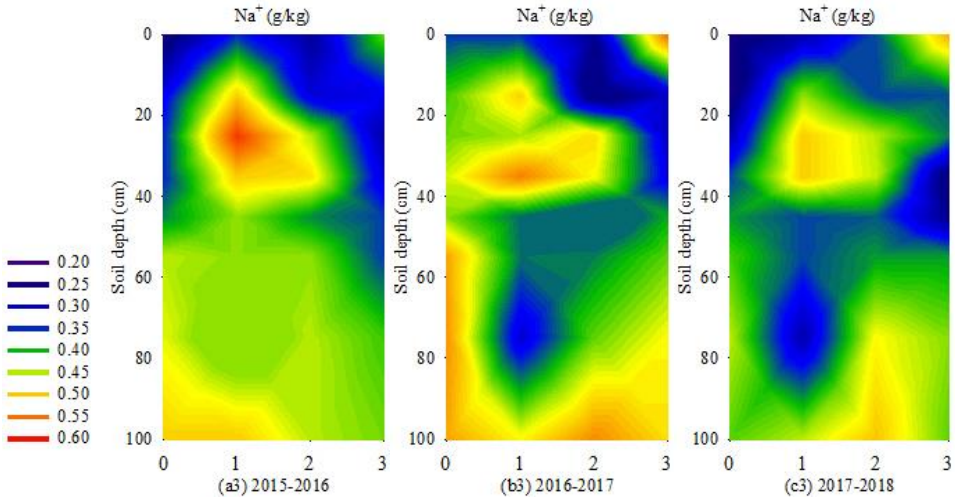

Figure 6: Distribution of cations in the 0–100 cm soil profile in 2015–2018

3.6 Changes (water:soil = 5:1) of SAR in the profile:

This study selected 2015-2016 as representative in the SAR analysis of the changes in the 0–100 cm soil layer (Table 4). SAR had significant differences ($P < 0.05$) in the 0–10, 10–20, 50–60 and 80–100 cm soil layers. In the 0–100 cm soil layer, SAR for BS, EFT, LFT and SA was 8.96–14.75, 10.01–13.61, 8.49–12.34 and 9.33–13.79 $(cmol \cdot kg^{-1})^{0.5}$, respectively. Thus, the Ca^{2+}, Mg^{2+} and Na^{+} contents of BS were redistributed in the 0–60 cm soil layer, thereby causing corresponding changes in SAR. The SAR of EFT was highest in the 20–30 cm soil layer. The SAR value of LFT increased with the increase in soil depth in the 0–40 cm soil layer, decreased and then increased in the 40–50 cm soil layer and decreased again in the 80–100 cm soil layer. The SAR of SA was higher [12.00 $(cmol \cdot kg^{-1})^{0.5}$] in the 0–10 cm soil layer and significantly lower [9.34 $(cmol \cdot kg^{-1})^{0.5}$] in the 10–30 cm soil layer. Subsequently, the SAR value increased with the increase in soil depth, reaching the maximum in the 80–100 cm soil layer [13.79 $(cmol \cdot kg^{-1})^{0.5}$]. The SAR of SA was larger in the 0–10 cm soil layer because Ca^{2+}, Mg^{2+} and Na^{+} content all increased, amongst which Na^{+} considerably increased.

Soil depth (cm)	BS	EFT	LFT	SA	SD	Sig.(2)	t
0-10	8.96	10.01	8.49	12.00	1.932	0.053	-2.167
10-20	11.44	12.42	9.01	9.34	2.114	0.041	-2.308
20-30	10.96	13.61	10.83	9.33	1.866	0.885	0.148
30-40	10.62	12.69	12.13	11.70	1.847	0.515	0.673
40-50	12.48	12.34	11.09	11.59	1.488	0.628	-0.498
50-60	14.75	11.22	12.03	12.35	1.999	0.182	1.424
60-80	11.11	10.81	12.34	13.15	2.325	0.526	0.654
80-100	12.17	13.28	11.77	13.79	1.176	0.012	2.994

BS: Before winter wheat sowing EFT: The early of freeze-thaw stage; LFT: The late of freeze-thaw stage; SA: the salt accumulation period; SD: Standard deviation; Sig. (2): Probability of two–sided test; t: The statistics of the test.

Table 4: Changes of SAR and its difference significance test in different soil layers in 2015-2016

4. Discussion

4.1 Effect of the freeze–thaw cycle on water movement

After a freeze–thaw cycle, the soil structure changes greatly due to the mechanical breaking of coarse particles and the aggregation of fine particles. In addition, soil particles condense and crystallise. Changing the particle size composition of mineral particles and structure in the soil strengthens particle adhesion and improves soil aggregate stability (Zhang *et al.*, 2016). During the destruction–reconstruction process, the pore water migrates from the warm end to the cold end under the driving of mass (Jambhekar *et al.*, 2015), momentum and energy exchange of soil and accumulates in the freezing front (Gray *et al.*, 1986). Under the conditions of this study, soil moisture migrates from the deep warm end to the cold surface in the EFT period. Accordingly, the spatial distribution of water shows a trend of large at both ends and small in the middle in the soil profile, that is, the 30–40 cm soil layer is divided and distributed up and down diversely. As temperatures rise, the thawing goes up and down at the same time. The unmelted soil layer in the middle blocks water and salt infiltration. Some of the soil water remaining in the upper layer moves to the surface layer under evaporation, whilst some continues to infiltrate with the melting soil layer. In the LFT stage, the 60–80 cm soil layer was taken as the boundary. The water content increased with soil depth in the 0–60 cm soil layer, whereas the water content in the soil layer below 80 cm increased compared with that in the 60–80 cm soil layer. The lower water content was due to the continued infiltration of water in the 60–80 cm soil layer, and the water above the 60 cm soil layer was not added in time because it was blocked by the unmelted soil layer. Soil water and salt movement were continuous and dynamic. However, the water and salt distribution obtained by sampling was static in this study, that was, only a fragment of water and salt movement under freezing–thawing conditions was intercepted. These soil layers were the middle layer of water conveyance, that was, 30–40 cm soil layer in the early stage of

freezing and 60–80cm soil layer in the late stage of freezing. The water content of the soil layer is lower than that of the adjacent upper and lower layers because the water transported upwards or to the lower layer has been exported, whereas the water supplied from the deep layer or from the upper layer is not yet in place. During the spring SA period, water was released into the atmosphere in the 0–20 cm soil layer, which was significantly lower than that below 20 cm soil layer. At this time, winter wheat roots were mostly concentrated in this soil layer, and spring irrigation should be implemented in time in accordance with the precipitation situation.

4.2 Effect of the freeze–thaw cycle on salt ion migration

Salt movement during the freeze–thaw cycle in soil was complicated. Such movement is affected by soil type, initial water content and salt content and type (Zhang *et al.*, 2005). Especially under field conditions, many influencing factors were considered (Li *et al.*, 2007). Increased salt content decreased thermal conductivity (Nidal *et al.*, 2000). Soil conductivity (EC) was directly related to these factors, that was, soil moisture content and the amount of dissolved salt in the soil. During the freezing process of soil, salt ion crystals reduce liquid water content and soil porosity, resulting in an upward pore blockage (Zhang *et al.*, 2005). Under the conditions of this study, salt ions (except HCO_3^-) accumulate above the 40 cm soil layer in the EFT stage, leading to the maximum soil EC appearing in the 20–30 cm soil layer. In the LFT period, all ions accumulate above the 40 cm or below the 60 cm soil layers. These comprehensive factors cause an inconsistency between the soil EC and the previous aggregation results in the surface layer (Wang *et al.*, 2009); however, these factors increased with soil depth. During the spring SA period, Cl^-, SO_4^{2-}, Ca^{2+} and Mg^{2+} all accumulate in the 0–20 cm soil layer, leading to the increase in soil EC in these layers. However, in terms of the entire soil layer, EC decreases due to the increase in the dispersion degree of soil and the decrease in hydraulic conductivity with the increase in SAR (Yadav *et al.*, 1981).

Stählia and Stadlerb (1997) found that soil salt undergoes freezing-induced redistribution. Firstly, the salt flows from the warm end to the cold end through convection. Secondly, the diffusion direction of salt is opposite to the development of concentration gradient. On the contrary, during the freeze–thaw process, salt moves vertically with water from surface to deep layer or vice versa (Gray *et al.*, 1986). However, the migration process of each ion was restricted by its solubility, temperature, channel connectivity and continuity (Fu *et al.*, 2016). Cl^- solubility was not affected by temperature; thus, it migrated to the cold end with water. The location of the lowest Cl^- content was in the 40–60 cm soil layer, which was determined by the largest frozen soil layer (61 cm) in the history of this region. The content of SO_4^{2-} increases further when it was near the cold end layer. In the EFT stage, the cooling property of SO_4^{2-} causes surface accumulation in the 10–30 cm soil layer. In the LFT period, the migration of SO_4^{2-} showed a distribution trend of large at both ends and small in the middle, that was, SO_4^{2-} accumulates in the top (20-40 cm) and deep layer (below 80 cm) layers. Cl^- and SO_4^{2-} migration leads to a chain change in the Cl^-/SO_4^{2-} ratio. In the EFT stage, the maximum ratio of Cl^-/SO_4^{2-} is in the 50–60 cm soil layer, whereas in the LFT stage, it is in the 30–40 cm soil layer.

In the EFT, SA and LFT periods, Na^+ showed a trend of large and small at both ends, that was, surface and deep layer accumulation coexist. In the EFT and LFT stages, Mg^{2+} shows a trend of large at both ends and small in the middle. In the EFT stage, Mg^{2+} accumulates at the surface (0–20 cm and below 60 cm soil layers). In the LFT stage, Mg^{2+} accumulates in the soil layer below 80 cm and at 30–40 cm simultaneously. Soil calcium content was an important parameter to evaluate soil properties (Yadav *et al.*, 1981). Ca^{2+} moved upward with water and accumulates in the 20–30 cm soil layer in the EFT period. In the LFT stage, surface and deep layer accumulation occur in the 10–40 and 80–100 cm soil layers, respectively. The sodium absorption ratio of soil was also considered to be an important chemical characteristic (Moasheri *et al*., 2013), and it was a good indicator for practical soil management, particularly in quantifying the amount of amendments (Zia *et al*., 2006). During the SA period, SAR decreased significantly (9.34) in the 10–30 cm soil layer, and then the SAR increased with the increase in soil depth, reaching the maximum in the 80–100 cm soil layer (13.79). Water and salt redistribution were beneficial to soil desalination in saline soil under the infiltration of salt in ice-melted water. This finding was consistent with the research results of Li *et al.* (2008). However, sodium could potentially cause soil structure deterioration and water infiltration problems (Abdulwahed *et al.*, 2016). Therefore, there should take some measure to reduce surface SA damage during the accumulation period in spring.

5. Conclusion

(1) Water moves from the warm side to the cold side under freeze–thaw conditions. In the EFT stage, soil moisture distribution is divided in the 30–40 cm soil layer boundary and shows a trend in which two ends are big, and the middle is small. In the LFT stage, soil water content increases with soil depth in the 0–60 cm soil layer; water content increases in the soil layer below 80 cm; and soil moisture content is lowest in the 60–80 cm soil layer.

(2) In the EFT stage, SO_4^{2-}, Cl^-, Mg^{2+} and Na^+ accumulate and coexist in the surface and deep layers; HCO_3^- accumulates in the 50–80 cm soil layer; and Ca^{2+} accumulates in the 20–30 cm soil layer. In the LFT period, SO_4^{2-}, Ca^{2+}, Mg^{2+} and Na^+ all show a trend in which two ends are big, and the middle is small; Cl^- accumulates in the soil layer below 60 cm, whereas HCO_3^- accumulates in the 0–30 cm soil layer.

(3) During the accumulation period in Spring, the moisture in the 0-20 cm soil layer was significantly lower than that in other soil layers. At the same time, various ions are concentrated in 0-20 cm soil layer. Therefore, spring irrigation should be timely conducted to alleviate the dual stress of drought and salt on crops.

In addition, soil water and salt movement are continuous and dynamic. This study used samples during critical periods to obtain the characteristic data of water and salt movement under freeze–thaw conditions. Further studies on the continuous movement law of water and salt under freeze–thaw conditions must be conducted.

Acknowledgements

The authors acknowledge the contributions of the National Natural Science Foundation of Key Projects of China (51790534), the National Key Research and Development Plan of China (2018YFD0300505) and

the system innovation team of the wheat industry in Hebei Province, China.

References

1. Aboukarima AM, El-Marazky MS, Ghoneim AM, et al. Modelling of Sodium Adsorption Ratio of the Soil Using Adaptive Neuro Fuzzy Inference System. Journal of Experimental Agriculture International (2016): 1-2.
2. Lundberg A, Ala-Aho P, Eklo O, et al. Snow and frost: implications for spatiotemporal infiltration patterns–a review. Hydrological processes 30 (2016): 1230-1250.
3. Asare SN, Rudra RP, Dickinson WT, et al. Effect of freeze–thaw cycle on the parameters of the Green and Ampt infiltration equation. Journal of agricultural engineering research 73 (1999): 265-274.
4. Bao SD. Soil and Agricultural Chemistry Analysis 2000.
5. Bryan BA, Gao L, Ye Y, et al. China's response to a national land-system sustainability emergency. Nature 559 (2018): 193-204.
6. Chapra SC. Surface Water-Quality Modeling (Illinois) (1997).
7. Hao C, Yali Y. Effect of Freezing and Thawing on Soil Compaction Under Pre-winter Irrigation in Northern China. Journal of Agricultural Mechanization Research 10 (2010).
8. Wagner-Riddle C, Congreves KA, Abalos D, et al. Globally important nitrous oxide emissions from croplands induced by freeze–thaw cycles. Nature Geoscience 10 (2017): 279-283.
9. Edwards AC, Cresser MS. Freezing and its effect on chemical and biological properties of soil. InAdvances in soil science (1992): 59-79.
10. Fouli Y, Cade-Menun BJ, Cutforth HW. Freeze–thaw cycles and soil water content effects on infiltration rate of three Saskatchewan soils. Canadian Journal of Soil Science 93 (2013): 485-496.
11. Qiang F, Renije H, Tianxiao L, et al. Soil moisture-heat transfer and its action mechanism of freezing and thawing soil. Trans. Chin. Soc. Agric. Mach 47 (2016): 99-110.
12. Gray DM, Granger RJ. In situ measurements of moisture and salt movement in freezing soils. Canadian Journal of Earth Sciences 23 (1986): 696-704.
13. Guo ZQ, Zhou YL, Zhang RJ, et al. Salt such soil potential analysis in Hebei and development exploitation. Proceedings of the annual conference of Chinese society of agricultural resources and regionalization (2012).
14. He HL. Application of Time Domain Reflectometry and Heat Pulse Methods for Quantifying Phase Change, Water Flow and Heat Transport in Frozen Soils (2005).
15. Jambhekar VA, Helmig R, Schröder N, et al. Free-flow–porous-media coupling for evaporation-driven transport and precipitation of salt in soil. Transport in Porous Media 110 (2015): 251-280.
16. Ren J, Vanapalli SK. Comparison of Soil-Freezing and Soil-Water Characteristic Curves of Two Canadian Soils. Vadose Zone Journal 18 (2019).

17. Gui-Yuan LI, Hao-Ming FA. Effect of freeze-thaw on water stability of aggregates in a black soil of Northeast China. Pedosphere 24 (2014): 285-290.
18. Ruiping L, Haibin S, Akae T. Characteristics of air temperature and water-salt transfer during freezing and thawing period. Transactions of the Chinese Society of Agricultural Engineering 2007 (2007).
19. Li Z, Liu X, Zhang X, et al. Infiltration of melting saline ice water in soil columns: Consequences on soil moisture and salt content. Agricultural water management 95 (2008): 498-502.
20. Ma W, Mao Z, Yu Z, et al. Effects of saline water irrigation on soil salinity and yield of winter wheat–maize in North China Plain. Irrigation and Drainage Systems 22 (2008): 3-18.
21. Miao C, Chen J, Zheng X, et al. Soil water and phreatic evaporation in shallow groundwater during a freeze–thaw period. Water 9 (2017): 396.
22. Moasheri SA, Foroughifar H. Estimation of the values of soil absorption ratio using integrated geostatistical and artificial neural network methods. International Journal of Agriculture and Crop Sciences (IJACS) 5 (2013): 2423-2433.
23. Seilsepour M, Rashidi M, Khabbaz BG. Prediction of soil exchangeable sodium percentage based on soil sodium adsorption ratio. American-Eurasian Journal of Agricultural and Environmental Sciences 5 (2009): 1-4.
24. Abu-Hamdeh NH, Reeder RC. Soil thermal conductivity effects of density, moisture, salt concentration, and organic matter. Soil science society of America Journal 64 (2000): 1285-1290.
25. Rozelle S, Veeck G, Huang J. The impact of environmental degradation on grain production in China, 1975–1990. Economic Geography 73 (1997): 44-66.
26. Shi M, Gao Z, Wan L, et al. Desalination of saline groundwater by a weakly permeable clay stratum: a case study in the North China Plain. Environmental Earth Sciences 78 (2019): 547.
27. Song Y, Zou Y, Wang G, et al. Altered soil carbon and nitrogen cycles due to the freeze-thaw effect: A meta-analysis. Soil Biology and Biochemistry 109 (2017): 35-49.
28. Spiess A. Developing adaptive capacity for responding to environmental change in the Arab Gulf States: Uncertainties to linking ecosystem conservation, sustainable development and society in authoritarian rentier economies. Global and Planetary Change 64 (2008): 244-252.
29. Stähli M, Stadler D. Measurement of water and solute dynamics in freezing soil columns with time domain reflectometry. Journal of Hydrology 195 (1997): 352-369.
30. Tilman D, Cassman KG, Matson PA, et al. Agricultural sustainability and intensive production practices. Nature 418 (2002): 671-677.
31. Wang WZ, Wu YR, Jin R, et al. Analysis of the Variation Characteristics of Soil Moisture and Soil Salinity——Take Arou Pasture in the Upper Reaches of Heihe River for an Example. Journal of Glaciology and Geocryology (2009).

32. Wang X, Wang C, Wang X, et al. Response of soil compaction to the seasonal freezing-thawing process and the key controlling factors. Catena 184 (2020): 104247.
33. Warren JK. Salt dissolution and pointers to vanished evaporites: Karst, breccia, nodules and cement. InEvaporites (2016): 613-761.
34. Wertz S, Goyer C, Zebarth BJ, et al. The amplitude of soil freeze-thaw cycles influences temporal dynamics of N 2 O emissions and denitrifier transcriptional activity and community composition. Biology and Fertility of Soils 52 (2016): 1149-1162.
35. Wu M, Tan X, Huang J, Wu J, Jansson PE. Solute and water effects on soil freezing characteristics based on laboratory experiments. Cold Regions Science and Technology 115 (2015): 22-29.
36. Xu, X, Wang, J and Zhang, L. Frozen soil physics. *Science Press* (2010).
37. Yadav JS, Girdhar IK. The effects of different magnesium: calcium ratios and sodium adsorption ratio values of leaching water on the properties of calcareous versus noncalcareous soils. Soil Science 131 (1981): 194.
38. Yan G, Xing Y, Xu L, et al. Nitrogen deposition may enhance soil carbon storage via change of soil respiration dynamic during a spring freeze-thaw cycle period. Scientific reports 6 (2016): 1-9.
39. Yi J, Zhao Y, Shao MA, et al. Soil freezing and thawing processes affected by the different landscapes in the middle reaches of Heihe River Basin, Gansu, China. Journal of hydrology 519 (2014): 1328-1338.
40. Zhang DF, Zheng QH, Dong ZY. Mechanism of soil salt-moisture transfer under freeze-thawing condition. Bull. Soil Water Conserv 25 (2005): 14-18.
41. Zhang X, Li P, Li ZB, et al. Soil water-salt dynamics state and associated sensitivity factors in an irrigation district of the loess area: a case study in the Luohui Canal Irrigation District, China. Environmental Earth Sciences 76 (2017): 715.
42. Zhang Z, Wei MA, Wenjie FE, et al. Reconstruction of soil particle composition during freeze-thaw cycling: a review. Pedosphere 26 (2016): 167-179.
43. Zia MH, Ghafoor A, Murtaza G, et al. Growth response of rice and wheat crops during reclamation of saline-sodic soils. Pakistan Journal of Botany 38 (2006): 249-266.